Eur. Phys. J. D **45**, 235–246 (2007)
DOI: 10.1140/epjd/e2007-00274-6

THE EUROPEAN PHYSICAL JOURNAL D

Lifetime vibrational interference during the NO $1s^{-1}\pi^*$ resonant excitation studied by the $NO^+(A\ ^1\Pi \rightarrow X\ ^1\Sigma^+)$ fluorescence

A. Ehresmann[1], W. Kielich[1], L. Werner[1], Ph.V. Demekhin[1,2], D.V. Omel'yanenko[2], V.L. Sukhorukov[2,3,a], K.-H. Schartner[4], and H. Schmoranzer[5]

[1] Institute of Physics and CINSaT, University of Kassel, 34132 Kassel, Germany
[2] Rostov State University of Transport Communications, 344038 Rostov-on-Don, Russia
[3] Institute of Physics, Southern Federal University, 344090 Rostov-on-Don, Russia
[4] I. Institute of Physics, Justus-Liebig University Giessen, 35392 Giessen, Germany
[5] Department of Physics, Kaiserslautern University of Technology, 67653 Kaiserslautern, Germany

Received 17 April 2007 / Received in final form 6 July 2007
Published online 26 September 2007 –

Abstract. Dispersed fluorescence from fragments formed after the de-excitation of the $1s^{-1}\pi^*$ resonances of N^*O and NO^* has been measured in the spectral range of 118–142 nm. This range is dominated by lines of atomic nitrogen and oxygen fragments and by the $A\ ^1\Pi\,(v') \rightarrow X\ ^1\Sigma^+\,(v'')$ bands in the NO^+ ion which result from the participator Auger decay of the $1s^{-1}\pi^*$ resonances. Ab-initio calculations of the transition probabilities between vibrational levels during the reaction NO $X\ ^2\Pi\,(v_0 = 0) \rightarrow N^*O(NO^*)\ 1s^{-1}\pi^*\,(v_r) \Longrightarrow NO^+\ A\ ^1\Pi\,(v') \rightarrow X\ ^1\Sigma^+\,(v'')$ were used to explain the observed intensity dependence for the $A\,(v') \rightarrow X\,(v'')$ fluorescence bands on the exciting-photon energy across the resonances and on both v' and v'' vibrational quantum numbers. The multiplet structure of the $1s^{-1}\pi^*$ resonance and lifetime vibrational interference explain the observed exciting-photon energy dependence of the $A\,(v') \rightarrow X\,(v'')$ fluorescence intensity. A strong spin-orbit coupling between singlet and triplet states of NO^+ is proposed to reduce additional cascade population of the $A\ ^1\Pi$ state via radiative transitions from the $W\ ^1\Delta$ and $A'\ ^1\Sigma^-$ states and to explain remaining differences between measured and calculated integral fluorescence intensities.

PACS. 32.80.Hd Auger effect and inner-shell excitation or ionization – 33.80.-b Photon interactions with molecules – 33.50.Dq Fluorescence and phosphorescence spectra

1 Introduction

The interference between the excitation pathways of molecules via different vibrational levels of an intermediate electronic state known as the lifetime vibrational interference (LVI) had been predicted almost 30 years ago [1]. Since then the LVI has been extensively studied in a number of papers (see, e.g., the review [2]). Strong LVI in recorded spectra is expected when the widths of the short-lived intermediate vibronic states, Γ_r, are comparable with their energetic spacing, characterized by the vibrational constant ω_e. In the case of the $1s^{-1}\pi^*$ resonance in the O_2 molecule the ratio $\Gamma_r/\omega_e \sim 1.10$ (0.149 eV/0.135 eV [3,4]) and the influence of the LVI on measured Auger decay spectra had been found to be strong [4]. In the N_2 molecule this ratio is half as large $\Gamma_r/\omega_e \sim 0.49$ (0.115 eV/0.235 eV [3,5]). That causes a relatively small influence of the LVI on the $A, B(v') \rightarrow X(v'')$ [6] and $C(v') \rightarrow X(v'')$ [7,8] fluorescence of the N_2^+ ion, where the initial states A, B and C of the N_2^+ have been populated via the $1s^{-1}\pi^*$ resonance of the N_2.

The NO molecule is of special interest for studying the LVI because the same ionic states can be accessed via the $1s^{-1}\pi^*$ resonance excitation of either N^*O or NO^*. The ratios Γ_r/ω_e of these resonances are equal to 0.64 (0.124 eV/0.195 eV [9]) and 1.13 (0.170 eV/0.150 eV [10]), respectively. Therefore, the differing influence of the LVI on the decay spectra of the $1s^{-1}\pi^*$ resonances of N^*O (small influence) or NO^* (large influence) has been observed by different experimental techniques. The decay of core-excited N^*O and NO^* resonances has been studied by measuring the resonant Auger electron spectra [11–14], vibrationally resolved constant ionic state spectra (CIS) [9, 15] and mass-selective ion-yield (photofragmentation) spectra [16,17]. The electronic part of the Auger decay of the $1s^{-1}\pi^*(^2\Lambda)$ resonances in NO has been computed by [18]. In studying the LVI by means of electron spectroscopy only, the energetic overlaps between the core-excited $1s^{-1}\pi^*(^2\Lambda)$ resonances and between the

[a] e-mail: vls@rgups.ru

valence-ionized states cause substantial difficulties in the interpretation of spectra and in the quantitative comparison with calculations (see, e.g., [14]). However, by observing the molecular fluorescence from the excited valence-ionized states, complementary information about LVI can be obtained since this fluorescence is state selective [6–8].

Recently, we have investigated the $C\ ^2\Sigma_u^+ \rightarrow X\ ^2\Sigma_g^+$ fluorescence in the N_2^+ ion excited via the $1s^{-1}\pi^*$ resonance [7,8]. Strongly overlapping $C(v') \rightarrow X(v'')$ bands characterized by the same difference of the vibrational quantum numbers $\Delta v = v' - v''$ were observed in [7] due to the small difference between the vibronic constants of the C and X states of N_2^+. This overlap requires ultra-high fluorescence resolution in order to observe the influence of the LVI on the fluorescence spectra of the N_2^+. In the case of the $A\ ^1\Pi \rightarrow X\ ^1\Sigma^+$ fluorescence in the NO^+ ion it is possible to distinguish individual bands since the vibrational constants ω_e of the A and X states of NO^+ are quite different (1601.9 cm^{-1} and 2376.7 cm^{-1}, respectively, [19]). Therefore, it is expected that the influence of the LVI on the individual $A(v') \rightarrow X(v'')$ bands even in relatively low resolution emission spectra (e.g. $\Delta\lambda_{fl} \sim 0.73$ nm in [20]) can be observed.

The $NO^+(A\ ^1\Pi \rightarrow X\ ^1\Sigma^+)$ fluorescence (known as the 'Miescher-Baer' band system [21]) is one of the most thoroughly studied band system in the NO^+ ion. Since the observation of this fluorescence in an uncondensed discharge in [22] and its interpretation in [23,24] it was revisited several times in [25–28] in order to determine the vibrational and rotational constants of the A and X states of the NO^+. Vibrational structure of valence-ionized $5\sigma^{-1}2\pi\left(^{1,3}\Pi\right)$ and $1\pi^{-1}2\pi\left(^{1,3}\Sigma^{\pm},\Delta\right)$ states of the NO^+ ion including the A and X ones was studied in numerous experimental papers by means of photoelectron spectroscopy (PES) [29–32] and photoabsorption/photoionization spectroscopy (see, e.g., [33] and references therein). The potential energy curves of the NO^+ states were calculated in [34,35].

In the present paper we report a joint experimental and theoretical study of the lifetime vibrational interference in the $1s^{-1}\pi^*$ resonant excitation of the N^*O and NO^* molecule by means of the $A\ ^1\Pi \rightarrow X\ ^1\Sigma^+$ fluorescence in the NO^+ ion. The obtained results are presented similarly to our previous study of the $N_2^+\left(C\ ^2\Sigma_u^+ \rightarrow X\ ^2\Sigma_g^+\right)$ fluorescence [7,8]. The paper is organized as follows. The essentials of the measurements and of the data analysis are described in Section 2. In Section 3 we continue with the brief presentation of the theoretical approach used in computing the molecular de-excitation dynamics for the Auger decay and the subsequent fluorescence emission. Experimental and theoretical results are discussed and compared in Section 4. In Section 5 we conclude with a brief summary.

2 Experiment

Photon-induced fluorescence spectroscopy (PIFS) has already been applied for several experiments investigating de-excitation of excited molecules [7,8,36–38]. The present experimental setup is quite similar to these experiments and has been described in detail elsewhere (see, e.g., [39–41] and references therein). Therefore, only the essential points of the present experiment will be described below.

The experiment was performed at the UE 56/2 PGM beamline at BESSY II, Berlin. A 400 lines/mm grating was used to monochromatize the synchrotron radiation which was then focused into a differentially pumped target cell filled with molecular nitric oxide at room temperature and at a pressure of 33.3 μbar. The pressure was chosen to be in the linear regime of the fluorescence intensity-pressure function, to avoid artifacts such as photoelectron-impact induced fluorescence. The exciting-photon energy was varied around the $N^*O(1s^{-1}\pi^*)$ resonance from 398.95 eV to 400.85 eV and around the $NO^*(1s^{-1}\pi^*)$ resonance from 530.90 eV to 535.45 eV in steps of 50 meV. A bandwidth of the exciting radiation of about 100 meV FWHM at 400 eV and 135 meV at 530 eV was achieved in order to be in the Raman regime for resonance excitation since the natural widths of the N^*O and NO^* resonances are 124 meV [9] and 170 meV [10], respectively. The exciting-photon energy was calibrated to the known [9,10] energy positions of the $1s^{-1}\pi^*(v_r)$ vibrational levels.

Fluorescence radiation between 118 and 142 nm was observed perpendicular to the exciting-photon beam and parallel to the $\overrightarrow{E}$-vector of the linearly polarized exciting radiation. The fluorescence was dispersed by a 1 m normal-incidence monochromator equipped with a 1200 lines/mm grating (blaze wavelength: 150 nm; coating: Al) and recorded by a position-sensitive CsI microchannel-plate detector. The resolution of this 'monochromator-detector' combination was about $\Delta\lambda_{fl} =$ 0.2 nm.

Two-dimensional fluorescence yield spectra in the fluorescence wavelength range from 118 to 142 nm and in the exciting-photon energy ranges around the N^*O resonance (398.95–400.85 eV) and the NO^* resonance (530.90–535.45 eV) are displayed in Figures 1 and 2, respectively. Figures 1a and 2a show the counts recorded by the present fluorescence detector, normalized for the exciting-photon flux. These counts have still not been corrected for the quantum efficiency of the fluorescence spectrometer-detector combination. The quantum efficiency (QE) of the CsI detector equipped with a MgF_2 window specified by its manufacturer (ITT) is given in Figures 1c and 2c. However, in this curve the reflectivity variation of the Al coating of the grating, the relative lateral quantum efficiency of the detector and the blaze angle distribution function (grating blazed at 150 nm) were neglected. The variation of these quantities is estimated to contribute an uncertainty of about 5% to the relative fluorescence intensities.

Assignments of the fluorescence lines observed between 118 and 142 nm are listed in Table 1. The numbering of lines corresponds to Figures 1b and 2b where the intensities integrated over the present exciting-photon energies are also shown. The NI, NII and OI atomic lines have been assigned by comparing the experimentally determined

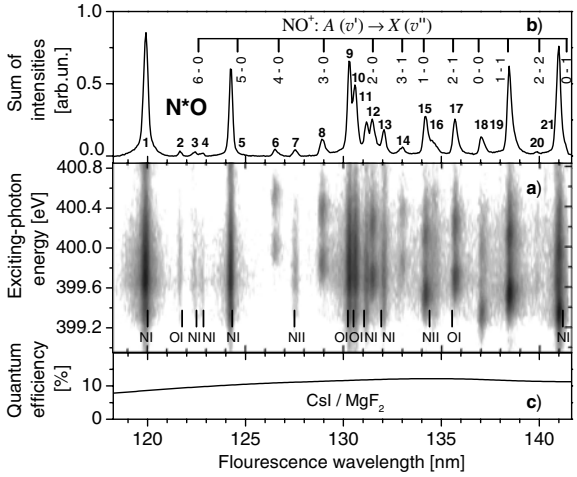

Fig. 1. The fluorescence spectrum measured in the vicinity of the N*O resonance (398.95–400.85 eV) and in the fluorescence wavelength range from 118 to 142 nm. (a) Dispersed fluorescence yield as a function of the exciting-photon energy with indicated positions of lines corresponding to transitions in NI, NII and OI fragments. (b) Fluorescence intensities integrated over the present exciting-photon energy range. Computed positions of the NO^+ $(A-X)$ vibrational bands are shown by vertical bars. Numbering of lines and their assignments as listed in Table 1. (c) Quantum efficiency of the CsI detector with MgF_2 window as specified by the manufacturer ITT.

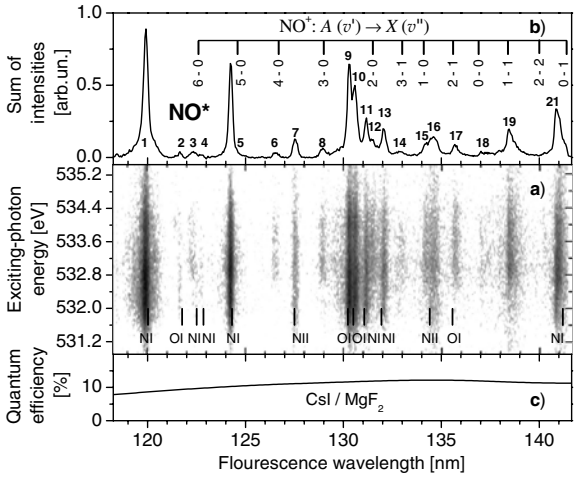

Fig. 2. The fluorescence spectrum measured in the vicinity of the NO* resonance (530.90–535.45 eV) and in the fluorescence wavelength range from 118 to 142 nm. Notations are the same as in Figure 1.

wavelengths with known spectroscopic data [42]. Wavelengths of the NO^+ fluorescence lines in the second column, λ_{exp}, were determined in the present paper by fitting the measured line shapes by Voigt profiles. They are in a good agreement with the experimental fluorescence wavelengths from [19,20,23]. The small difference between our experimentally determined λ_{exp} for line No. 21 (140.9 nm) and data known from the literature (141.4 nm [19,20, 23]) which is larger than the present fluorescence wavelength uncertainty, $\Delta\lambda_{fl} = 0.2$ nm, is due to the non-

Table 1. Assignment of the observed fluorescence lines after resonant $1s^{-1}\pi^*$ excitation in NO. The numbers in the first column correspond to the line numbering in Figures 1b and 2b.

No.	$\lambda^{a)}_{exp}$ nm	$\lambda^{b)}_{calc}$ nm	Species	Transition		
1	120.0		NI	$2s^22p^2(^3\mathrm{P})3s\,^4\mathrm{P}_{J'}$	$\rightarrow$	$2s^22p^3\,^4\mathrm{S}_{J''}$
2	121.8		OI	$2s^22p^3(^2\mathrm{P})3s\,^1\mathrm{P}_1$	$\rightarrow$	$2s^22p^4\,^1\mathrm{S}_0$
3	122.5		NI	$2s^22p^2(^3\mathrm{P})4d\,^2\mathrm{D}_{J'}$	$\rightarrow$	$2s^22p^3\,^2\mathrm{P}_{J''}$
		122.6	NO^+	$A\,^1\Pi(v'=6)$	$\rightarrow$	$X\,^1\Sigma^+(v''=0)$
4	122.9		NI	$2s^22p^2(^3\mathrm{P})4d\,^2\mathrm{P}_{J'}$	$\rightarrow$	$2s^22p^3\,^2\mathrm{P}_{J''}$
5	124.3		NI	$2s^22p^2(^1\mathrm{D})3s\,^2\mathrm{D}_{J'}$	$\rightarrow$	$2s^22p^3\,^2\mathrm{D}_{J''}$
		124.6	NO^+	$A\,^1\Pi(v'=5)$	$\rightarrow$	$X\,^1\Sigma^+(v''=0)$
6	126.5	126.7	NO^+	$A\,^1\Pi(v'=4)$	$\rightarrow$	$X\,^1\Sigma^+(v''=0)$
7	127.5		NII	$2s^22p^1(^2\mathrm{P})3p\,^3\mathrm{P}_2$	$\rightarrow$	$2s^12p^3\,^3\mathrm{D}_3$
8	128.9	129.0	NO^+	$A\,^1\Pi(v'=3)$	$\rightarrow$	$X\,^1\Sigma^+(v''=0)$
9	130.2		OI	$2s^22p^3(^4\mathrm{S})3s\,^3\mathrm{S}_1$	$\rightarrow$	$2s^22p^4\,^3\mathrm{P}_2$
10	130.6		OI	$2s^22p^3(^4\mathrm{S})3s\,^3\mathrm{S}_1$	$\rightarrow$	$2s^22p^4\,^3\mathrm{P}_{0,1}$
11	131.1		NI	$2s^22p^2(^3\mathrm{P})3d\,^2\mathrm{D}_{J'}$	$\rightarrow$	$2s^22p^3\,^2\mathrm{P}_{J''}$
12	131.4	131.5	NO^+	$A\,^1\Pi(v'=2)$	$\rightarrow$	$X\,^1\Sigma^+(v''=0)$
13	131.9		NI	$2s^22p^2(^3\mathrm{P})3d\,^2\mathrm{P}_{J'}$	$\rightarrow$	$2s^22p^3\,^2\mathrm{P}_{J''}$
14	133.0	133.0	NO^+	$A\,^1\Pi(v'=3)$	$\rightarrow$	$X\,^1\Sigma^+(v''=1)$
15	134.1	134.1	NO^+	$A\,^1\Pi(v'=1)$	$\rightarrow$	$X\,^1\Sigma^+(v''=0)$
16	134.4		NII	$2s^22p^1(^2\mathrm{P})3p\,^3\mathrm{D}_{J'}$	$\rightarrow$	$2s^12p^3\,^3\mathrm{D}_{J''}$
17	135.6	135.6	NO^+	$A\,^1\Pi(v'=2)$	$\rightarrow$	$X\,^1\Sigma^+(v''=1)$
	135.7		OI	$2s^22p^3(^4\mathrm{S})3s\,^5\mathrm{S}_2$	$\rightarrow$	$2s^22p^4\,^3\mathrm{P}_{0,1}$
18	137.0	136.9	NO^+	$A\,^1\Pi(v'=0)$	$\rightarrow$	$X\,^1\Sigma^+(v''=0)$
19	138.4	138.4	NO^+	$A\,^1\Pi(v'=1)$	$\rightarrow$	$X\,^1\Sigma^+(v''=1)$
20	139.8	140.0	NO^+	$A\,^1\Pi(v'=2)$	$\rightarrow$	$X\,^1\Sigma^+(v''=2)$
21	140.9	141.4	NO^+	$A\,^1\Pi(v'=0)$	$\rightarrow$	$X\,^1\Sigma^+(v''=1)$
		141.7	NO^+	$A\,^1\Pi(v'=3)$	$\rightarrow$	$X\,^1\Sigma^+(v''=3)$
	141.2		NI	$2s^22p^2(^1\mathrm{D})3s\,^2\mathrm{D}_{J'}$	$\rightarrow$	$2s^22p^3\,^2\mathrm{P}_{J''}$

[a)] Wavelength for the transitions in NO^+, present measurement; for the NI, OI and NII atomic fluorescence the wavelengths are averaged over the fine-structure components [42]; [b)] wavelength for the transitions in NO^+, present calculations.

linearity of the microchannel-plate position-sensitive detector near its edge. The theoretical wavelengths of the $A\,^1\Pi(v') \rightarrow X\,^1\Sigma^+(v'')$ vibrational bands, λ_{calc}, are also shown in the Figures 1b, 2b and listed in the third column of Table 1.

The observed atomic fluorescence provides information on the probabilities of the dissociative Auger decay and the dissociative double Auger decay of the $1s^{-1}\pi^*$ resonance. However, the precise interpretation of the above processes requires extensive computation of potential energy curves for highly-excited states of NO, NO^+ and NO^{2+} and is outside the scope of the present paper. In the present paper we concentrate on the interpretation of the molecular fluorescence observed for the NO^+ ion.

One can see that the 6→0, 5→0 and 0→1 bands of the $A \rightarrow X$ system are blended by atomic transitions (see ambiguous assignment of lines nos 3, 5 and 21 listed in Tab. 1), whereas the well separated but weak 2→2 band in the NO* case could not be resolved in the present experiment. All other bands of the $A\,^1\Pi \rightarrow X\,^1\Sigma^+$ system were resolved and possess nontrivial intensity variations with the exciting-photon energy across the resonances. In order to analyze the observed energy dependence of the fluorescence intensities we introduced the integrated cross sections similar to our previous papers [7,8]. Relative

integrated cross sections for the $A\ ^1\Pi(v') \rightarrow X\ ^1\Sigma^+(v'')$ bands at a given exciting-photon energy, $\sigma_{Av'}^{Xv''}(\omega)$, have been determined by integrating the fluorescence intensities, $I(\omega,\lambda)$, corrected for the QE of the detector over a wavelength interval of 0.4 nm centered at the wavelength $\lambda_{exp}^{v',v''}$ as listed in Table 1:

$$\sigma_{Av'}^{Xv''}(\omega) = \int_{\lambda_{exp}^{v',v''}-0.2\ \mathrm{nm}}^{\lambda_{exp}^{v',v''}+0.2\ \mathrm{nm}} I(\omega,\lambda)\ \mathrm{d}\lambda. \quad (1)$$

In order to analyze the total intensities of the $A(v') \rightarrow X(v'')$ bands we used the relative doubly integrated emission cross sections, $\bar{\sigma}_{Av'}^{Xv''}$, defined as:

$$\bar{\sigma}_{Av'}^{Xv''} = \int_{\omega_1}^{\omega_2} \sigma_{Av'}^{Xv''}(\omega)\ \mathrm{d}\omega, \quad (2)$$

where the exciting-photon energy range $(\omega_1 - \omega_2)$ corresponds either to the N^*O resonance (398.95–400.85 eV) or to the NO^* resonance (530.90–535.45 eV). The experimental cross sections $\sigma_{Av'}^{Xv''}(\omega)$ and $\bar{\sigma}_{Av'}^{Xv''}$ are discussed and compared with the present theory in Section 4.

3 Theory

In order to explain the $NO^+\left(A\ ^1\Pi \rightarrow X\ ^1\Sigma^+\right)$ fluorescence intensity distribution observed in the present experiment we consider, as the first step, the direct population of the $5\sigma^1 1\pi^4 2\pi^1\ A\ ^1\Pi(v')$ states of the NO^+ ion from the $1\sigma^2 2\sigma^2 3\sigma^2 4\sigma^2 5\sigma^2 1\pi^4 2\pi^1\ X\ ^2\Pi\,(v=0)$ ground state of the NO molecule via Auger decay of the $1\sigma^1(2\sigma^1)2\pi^2\ ^2\Lambda\,(v_r)$ doublet states of the intermediate NO^* (N^*O) resonance:

$$X\ ^2\Pi\,(0) + \hbar\omega_{ex} \rightarrow 1\sigma^1(2\sigma^1)2\pi^2 \left\{ \begin{array}{ll} ^2\Sigma^- & (\mathbf{a}) \\ ^2\Delta & (\mathbf{b}) \\ ^2\Sigma^+ & (\mathbf{c}) \end{array} \right\} (v_r)$$
$$\Longrightarrow 5\sigma^1 1\pi^4 2\pi^1\ A\ ^1\Pi(v') + e^-, \quad (3)$$

where the single and double arrows denote electric-dipole and Coulomb interaction, respectively. The influence of additional cascade population of the NO^+ A $^1\Pi(v')$ states is estimated in Section 4.3. In the present calculations we neglect a possible coupling of the channels in the final state of the Auger decay (3) since the multiplet splitting of the intermediate states is at least by two orders of magnitude larger than their fine-structure splitting. Thus we assumed that the de-excitation pathways (3a–3c) via the different $1\sigma^1(2\sigma^1)2\pi^2\ ^2\Lambda$ ($^2\Lambda = {}^2\Sigma^-$, $^2\Delta$ or $^2\Sigma^+$) intermediate electronic states populate the $5\sigma^1 1\pi^4 2\pi^1\ A\ ^1\Pi$ electronic state via different Auger channels and, therefore, incoherently (see also discussion in [15]). However, the excitation pathways via different vibrational levels v_r of the particular $1\sigma^1(2\sigma^1)2\pi^2\ ^2\Lambda$ intermediate electronic state populate the $A\ ^1\Pi(v')$ levels in a coherent way (LVI).

The excited $A\ ^1\Pi(v')$ states can either fluoresce to the $5\sigma^2 1\pi^4 2\pi^0\ X\ ^1\Sigma^+(v'')$ states via the $2\pi \rightarrow 5\sigma$ transition ($\lambda_{00} \approx 137$ nm):

$$5\sigma^1 1\pi^4 2\pi^1\ A\ ^1\Pi(v') \rightarrow 5\sigma^2 1\pi^4 2\pi^0\ X\ ^1\Sigma^+(v'') + \frac{hc}{\lambda_{fl}}, \quad (4)$$

or, if energetically possible, to the $5\sigma^2 1\pi^3 2\pi^1\ A'\ ^1\Sigma^-(v'')$ and $5\sigma^2 1\pi^3 2\pi^1\ W\ ^1\Delta(v'')$ states via $1\pi \rightarrow 5\sigma$ transitions ($\lambda_{00} \approx 2450$ nm and $\lambda_{00} \approx 4950$ nm, respectively). Although the $NO^+\left(b\ ^3\Pi \rightarrow X\ ^1\Sigma^+\right)$ triplet–singlet dipole transitions, which are possible due to spin-orbital interaction, have been observed in [20], we neglect, in the first step, possible $A\ ^1\Pi \rightarrow\ ^3\Lambda$ transitions. The influence of spin forbidden dipole transitions is discussed in Section 4.3.

In order to compute the transition energies and amplitudes entering the schemes (3) and (4) we computed the potential energy curves and probabilities for the Auger and radiative decays by applying the theoretical approach described in details in [7,8,37,38]. A brief description of the approximations used for solving these problems can be found in the subsequent sections.

3.1 General relations

Fluorescence emission cross sections for the $A\ ^1\Pi(v') \rightarrow X\ ^1\Sigma^+(v'')$ transitions in the NO^+ ion were calculated by:

$$\sigma_{Av'}^{Xv''}(\omega) = \sigma_{Av'}(\omega)\ \chi_{Av'}^{Xv''}, \quad (5)$$

where ω is the energy of the exciting radiation, $\chi_{Av'}^{Xv''}$ is the fluorescence yield for the $A\ ^1\Pi(v') \rightarrow X\ ^1\Sigma^+(v'')$ transition and the total population cross section $\sigma_{Av'}(\omega)$ is the sum of the partial cross sections $\sigma_{Av'}^{\Lambda}(\omega)$ (where $^2\Lambda = {}^2\Sigma^-$, $^2\Delta$ or $^2\Sigma^+$) for population of the $A\ ^1\Pi(v')$ vibrational levels from the NO $X\ ^2\Pi\,(v=0)$ ground state via the particular $1\sigma^1(2\sigma^1)2\pi^2\ ^2\Lambda$ resonance of N^*O and NO^*:

$$\sigma_{Av'}(\omega) = \sum_{\Lambda} \sigma_{Av'}^{\Lambda}(\omega). \quad (6)$$

The cross sections $\sigma_{Av'}^{\Lambda}(\omega)$ were computed as in [7]:

$$\sigma_{Av'}^{\Lambda}(\omega) = \frac{4}{3}\pi^2 \alpha a_0^2 \omega \times \sum_{\beta} \left| \sum_{v_r} \frac{\left\langle v' \left| \mathbf{V}_{\pi^*(\Lambda)}^{A\beta\varepsilon}(R) \right| v_r \right\rangle \left\langle v_r \left| \mathbf{D}_0^{\pi^*(\Lambda)}(R) \right| 0 \right\rangle}{\omega - E_{(\Lambda)v_r} + \imath \cdot \Gamma_{\pi^*(\Lambda)}/2} \right|^2, \quad (7)$$

where the length form is used for the dipole transition operator $\mathbf{D}$, $\alpha = 1/137.036$ is the fine structure constant, and the square of the Bohr radius $a_0^2 = 28.0028$ Mb converts the atomic units for cross sections to Mb (1 Mb = 10^{-22} m^2). The energy ω in equation (7) is connected with the energy of the Auger electron, ε, and the energy of the $A\ ^1\Pi(v')$ state, $E_{Av'}$, as $\omega = E_{Av'} + \varepsilon$; and $E_{(\Lambda)v_r}$ – is the energy of the $1\sigma^1(2\sigma^1)2\pi^2\ ^2\Lambda\,(v_r)$ vibronic states. The natural widths of the $1\sigma^1(2\sigma^1)2\pi^2\ ^2\Lambda$ electronic states, $\Gamma_{\pi^*(\Lambda)}$, are connected with the Auger decay and are similar for the $^2\Sigma^-$, $^2\Delta$, $^2\Sigma^+$ states [9,10].

Equation (7) can be transformed neglecting the R-dependencies of the transition moments (e.g., by applying

the Franck-Condon approximation):

$$\sigma^{A}_{Av'}(\omega) = \frac{4}{3}\pi^2\alpha a_0^2\omega \left|\mathbf{D}_0^{\pi^*(\Lambda)}\right|^2 \sum_{\beta}\left|\mathbf{V}^{A\beta\varepsilon}_{\pi^*(\Lambda)}\right|^2 \times \left|\sum_{v_r}\frac{\langle v'|v_r\rangle\langle v_r|0\rangle}{\omega - E_{(\Lambda)v_r} + \imath\Gamma_{\pi^*(\Lambda)}/2}\right|^2. \quad (8)$$

The first sum over index β in equation (8) is proportional to the partial Auger rate for populating the final $A\ ^1\Pi$ electronic state from $1\sigma^1(2\sigma^1)2\pi^2\ ^2\Lambda$ resonances. In atomic units, $\Gamma^{A}_{\pi^*(\Lambda)}$ is given by:

$$\Gamma^{A}_{\pi^*(\Lambda)} = 2\pi\sum_{\beta}\left|\mathbf{V}^{A\beta\varepsilon}_{\pi^*(\Lambda)}\right|^2. \quad (9)$$

The second sum of the transition amplitudes over index v_r in equation (8) accounts for the interference between the population pathways via different vibrational levels v_r of intermediate resonance (LVI).

The fluorescence yield for the $A\ ^1\Pi(v') \rightarrow X\ ^1\Sigma^+(v'')$ transition $\chi^{Xv''}_{Av'}$ entering equation (5) was computed by:

$$\chi^{Xv''}_{Av'} = \frac{\Gamma^{Xv''}_{Av'}}{\sum_{K'',v''}\Gamma^{K''v''}_{Av'}} \quad (10)$$

where index K'' denotes possible fluorescence decay channels of the $A\ ^1\Pi$ state ($K'' = X\ ^1\Sigma^+$, $A'\ ^1\Sigma^-$ or $W\ ^1\Delta$). The fluorescence probability $\Gamma^{Xv''}_{Av'}$ (which equals the partial radiative width in atomic units) is given by [43]:

$$\Gamma^{Xv''}_{Av'} = \frac{4}{3\,g_A}\left(\frac{2\pi}{\lambda_{v'v''}}\right)^3 \left|\langle v''|\mathbf{D}^X_A(R)|v'\rangle\right|^2, \quad (11)$$

where $g_A = 2$ is the statistical weight of the $A\ ^1\Pi$ state.

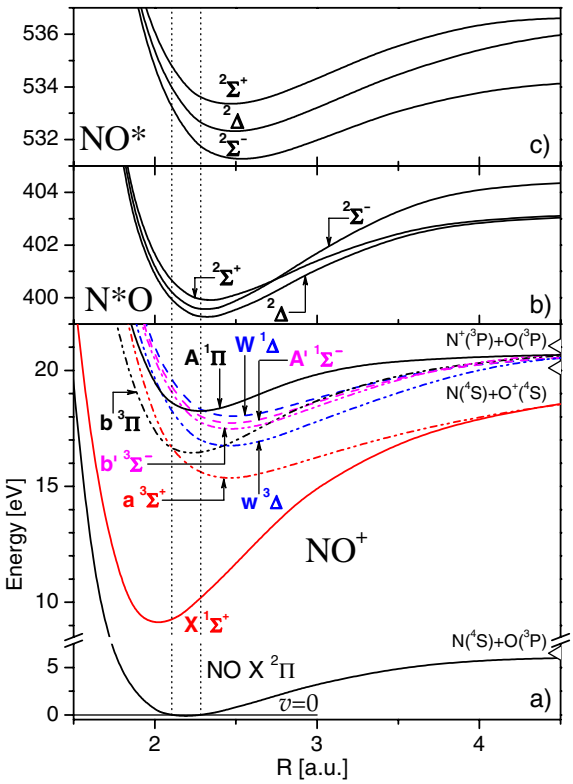

Fig. 3. (Color online) Present calculations. (a) Potential energy curves for the $X\ ^2\Pi$ ground state of the NO, and the $X\ ^1\Sigma^+$ and $A\ ^1\Pi$ states of NO^+ relevant to the present process (solid lines). Singlet $W\ ^1\Delta$, $A'\ ^1\Sigma^-$ and triplet $b'\ ^3\Sigma^-$, $w\ ^3\Delta$, $b\ ^3\Pi$, $a\ ^3\Sigma^+$ states of NO^+ are also shown by dash and dash-dot-dot lines, respectively. The dissociation limits are marked by hollow triangles and the Franck-Condon region for the ground state of NO is drawn in by vertical dot lines. (b) and (c) Potential energy curves for the $^2\Sigma^-$, $^2\Delta$ and $^2\Sigma^+$ states of core-excited N*O and NO* molecules simulated in the present work in the '$Z+1$' equivalent core approximation (see discussion in the text).

3.2 Molecular orbitals and potential curves

The adiabatic potential energy curves were computed similarly to our recent papers [7,37,38] using the PC GAMESS (General Atomic and Molecular Electronic Structure System) version Alex A. Granovsky (`www http://classic.chem.msu.su/gran/gamess/index.html`) of the GAMESS (US) QC package [44]. We used a triple-zeta valence (TZV) basis set [45] adding three polarization shells of d-type and one of f-type. A Multi Configuration Self Consistent Field (MCSCF) calculation choosing Full Valence Complete Active Space (FVCAS) with subsequent Multi Reference Configuration Interaction (MRCI) approach was applied to calculate the potential energy curves at a limited number of internuclear distances.

The results of calculations for the ground state of NO molecule and for some states of the NO^+ ion are presented in Figure 3 and compared with the results known from literature in Table 2. For the sake of compatibility between the data listed in Table 2 and those shown in Figure 3 the zero of the energy scale was set to the $v = 0$ vibrational level of the NO ground state and all the computed ionic potential curves of NO^+ were shifted by +0.35 eV. The latter shift was applied to eliminate the systematical difference originating from the different size of the virtual space used in the molecular ions CI calculations. Potential curves for the $X\ ^2\Pi$ ground state of NO, and the $X\ ^1\Sigma^+$ and $A\ ^1\Pi$ states of NO^+ relevant to the present process are drawn in by solid lines. To have a complete overview, the singlet $W\ ^1\Delta$, $A'\ ^1\Sigma^-$ (dash lines) and triplet $b'\ ^3\Sigma^-$, $w\ ^3\Delta$, $b\ ^3\Pi$, $a\ ^3\Sigma^+$ (dash-dot-dot lines) states of NO^+ are also shown. From Table 2 a good agreement between computed and measured [19,46] spectroscopic constants is obvious.

In order to compute the potential energy curves of the $^2\Sigma^-$, $^2\Delta$ and $^2\Sigma^+$ states of the N*O or NO* core-excited molecule we apply the equivalent core '$Z+1$' approximation. This approximation is rather restricted [47] and results, for instance, in a wrong order of the N*O electronic states [48]. Therefore we used experimental

Table 2. Comparison between experimental [19,46] and theoretical spectroscopic constants for the ground state of the NO molecule and some states of the NO^+ ion. Molecular constants D_0, ω_e, $\omega_e x_e$, r_e and IP_a have the standard meaning [19].

State/ Source	D_0 eV	ω_e cm^{-1}	$\omega_e x_e$ cm^{-1}	r_e Å	IP_a eV
NO X $^2\Pi$					
MRCI	6.15	1903	16.4	1.1586	
[19,46]	6.497	1904.2	14.08	1.1508	
NO^+ X $^1\Sigma^+$					
MRCI	10.64	2367	16.7	1.070	9.26
[19,46]	10.851	2376.7	16.26	1.0633	9.264
NO^+ a $^3\Sigma^+$					
MRCI	4.27	1273	15.3	1.298	15.63
[19,46]	4.452	1303.1	15.16	1.281	15.663
NO^+ b $^3\Pi$					
MRCI	4.38	1723	19.0	1.178	16.52
[19,46]	4.471	1710	14.18	1.1756	16.560
NO^+ w $^3\Delta$					
MRCI	4.09	1321	11.7	1.296	16.81
[19,46]	4.156	1316.9	10.83	1.279	16.875
NO^+ b′ $^3\Sigma^-$					
MRCI	3.36	1298	12.1	1.301	17.54
[19,46]	3.431	1283.2	10.77	1.2759	17.600
NO^+ A′ $^1\Sigma^-$					
MRCI	3.10	1278	13.5	1.299	17.80
[19,46]	3.212	1279.9	13.21	1.287	17.819
NO^+ W $^1\Delta$					
MRCI	2.81	1227	14.9	1.310	18.09
[19,46]	2.955	1217.7	11.59	1.301	18.076
NO^+ A $^1\Pi$					
MRCI	2.58	1567	16.5	1.203	18.32
[19,46]	2.705	1601.9	20.21	1.1939	18.325

photoionization spectra measured in [49] to calibrate the energies and equilibrium distances of the potential energy curves computed for the $X\ ^3\Sigma_g^-$, $a\ ^1\Delta_g$ and $b\ ^1\Sigma_g^+$ states of O_2 and the $X\ ^3\Sigma^-$, $a\ ^1\Delta$ and $b\ ^1\Sigma^+$ states of NF molecules.

Calculations were performed within the Franck-Condon approximation which influences the calculated photoionization spectra by no more than 5% [18]. The following parameters were used in the calculations: (i) the relative intensity ratios to excite the $^2\Sigma^+$, $^2\Delta$ and $^2\Sigma^-$ states of N*O (1.00:1.95:2.43) and NO* (1.00:2.13:3.52) from [18]; (ii) the natural widths of 124 meV [9] for N*O and 170 meV [10] for NO*; and (iii) the experimental [49] exciting-photons resolutions of 75 meV and 130 meV, respectively, for the N*O and NO* cases. The energies of the zero-vibrational levels of the $1\sigma^1(2\sigma^1)2\pi^2\ ^2\Lambda$ states, $E_{(\Lambda)v_r=0}$, and the shifts, $\Delta r_e(\Lambda)$, for the equilibrium internuclear distances, r_e^{calc}, calculated within the '$Z+1$' approximation were adjusted in the present work in order to reproduce the photoionization spectra from [49].

The total N*O and NO* photoionization cross sections calculated in the present work are compared with the experimental data measured by [49] in Figure 4. The contributions from transitions to the $^2\Sigma^-$, $^2\Delta$ and $^2\Sigma^+$ states are also shown. One can see a good overall agreement between computed and measured photoionization spectra

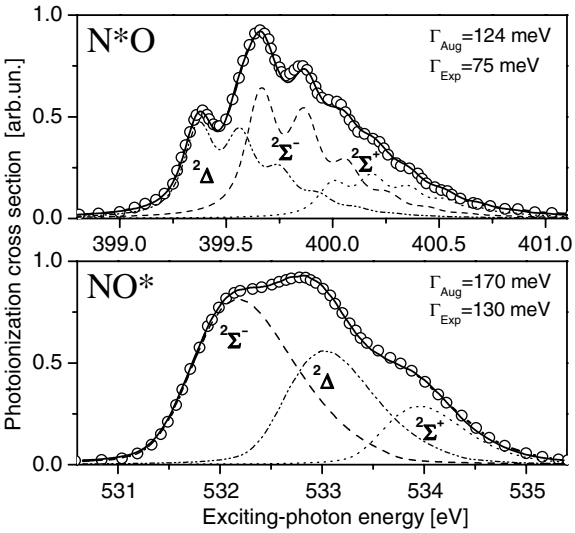

Fig. 4. Experimental N*O and NO* photoionization cross sections from [49] (open circles) together with presently computed ones (solid lines). The contributions from the transitions to the $^2\Sigma^-$ (dash), $^2\Delta$ (dash-dot-dot) and $^2\Sigma^+$ (dot) states are shown.

Table 3. Spectroscopic constants for the potential energy curves of N*O and NO* states calculated in the present work. Adjustments of both $r_e(\Lambda)$ and $E_{(\Lambda)v_r=0}$ for potential curves of the O_2 and NF molecules were made in order to reproduce the N*O and NO* photoionization spectra from [49].

State	E_0 eV	ω_e meV	$\omega_e x_e$ meV	$r_e^{*)}$ Å	$\Delta r_e^{*)}$ Å
N*O ($^2\Delta$)	399.37	194	1.9	1.228	+0.005
N*O ($^2\Sigma^-$)	399.66	203	1.6	1.224	+0.010
N*O ($^2\Sigma^+$)	400.00	184	2.1	1.235	+0.005
NO* ($^2\Sigma^-$)	531.33	150	1.5	1.340	+0.015
NO* ($^2\Delta$)	532.39	155	1.2	1.318	+0.005
NO* ($^2\Sigma^+$)	533.42	157	1.3	1.306	− 0.005

*) Listed values of the r_e are connected with the computed r_e^{calc} values and shifts $\Delta r_e(\Lambda)$ via equation $r_e = r_e^{calc} + \Delta r_e$.

depicted in Figure 4. The presently computed vibrational constants ω_e, $\omega_e x_e$ and adjusted values of $E_0 = E_{(\Lambda)v_r=0}$ and $r_e = r_e(\Lambda)$ (as well as the shifts $\Delta r_e = \Delta r_e(\Lambda)$) for potential energy curves of the N*O and NO* states are listed in Table 3. These constants are in good agreement with the experimental [9,10,49] and theoretical [18] data available from literature. The potential energy curves of the $^2\Sigma^-$, $^2\Delta$ and $^2\Sigma^+$ states of core-excited N*O and NO* molecule simulated in the present work are depicted in Figures 3b and 3c and used in the further calculations of the $A \to X$ fluorescence intensity distribution.

4 Results and discussion

In the following sections we analyze the fluorescence emission cross sections (1) and (2) measured in the present experiment. Therefore in Section 4.1 we compute cross sections for direct population of $A\ ^1\Pi\,(v')$ states via Auger

decay of N*O and NO* resonances. The experimental and theoretical cross sections for the NO^+ $\left(A\ ^1\Pi \rightarrow X\ ^1\Sigma^+\right)$ fluorescence are compared in Section 4.2. The influence of radiative cascade transitions in the NO^+ ion on the calculated fluorescence spectra is estimated in Section 4.3.

4.1 Direct population of the A $^1\Pi$ state

Partial $\sigma^A_{Av'}(\omega)$ and total $\sigma_{Av'}(\omega)$ cross sections for population of the $A\ ^1\Pi$ state via Auger decay of the N*O and NO* resonances were computed in the two approximations: with and without accounting for the LVI. Calculations were performed within the Franck-Condon approximation applying equation (8). We used the same intensity ratios to excite the $^2\Sigma^+$, $^2\Delta$ and $^2\Sigma^-$ states of N*O and NO* as in computing the photoionization cross section in Section 3.2. In order to compute the Auger rates (9) entering equation (8) the single center technique in combination with the MO LCAO technique was used as in our previous papers [7,38].

The relative partial Auger rates $\Gamma^A_{\pi^*(\Lambda)}$ calculated in the present work are 1.00:1.00:0.06 for the $^2\Sigma^+$,$^2\Delta$, $^2\Sigma^-$ states of the N*O resonance and 1.00:1.00:0.01, respectively, for the NO* resonance. These ratios are in good agreement with calculations of [18] which amount to 1.00: 0.92:0.12 for the $^2\Sigma^+$, $^2\Delta$, $^2\Sigma^-$ states of the N*O resonance and to 1.00:1.08:0.04, respectively, for the NO* resonance. The difference between these two calculations is connected with the fact that we used a single-electron HF approach for the final state of the molecular Auger transition whereas the CI approach and atomic integrals from the data tables of [50] have been applied by [18]. One can recognize that the partial Auger rate (9) for populating the $A\ ^1\Pi$ state via the $^2\Sigma^-$ resonance is almost by one order of magnitude smaller than the partial rates for the $^2\Delta$ and $^2\Sigma^+$ resonances which are practically equal. This is due to the destructive and constructive interference between direct, J, and exchange, K, Coulomb integrals entering the expressions for the $\mathbf{V}^{A\beta\varepsilon}_{\pi^*(\Lambda)}$ matrix elements $\left(\mathbf{V}^{A\beta\varepsilon}_{\pi^*(\Sigma^-)} \propto J-K \text{ and } \mathbf{V}^{A\beta\varepsilon}_{\pi^*(\Sigma^+,\Delta)} \propto J+K\right)$.

Total population cross sections $\sigma_{Av'}(\omega)$ computed for the $v' \leq 4$ vibrational levels relevant to the present measurements are depicted in Figure 5. In both cases, N*O and NO*, the partial cross sections $\sigma^A_{Av'}(\omega)$ are also shown in the uppermost panels for the $v'=0$ vibrational level only. One can recognize that the partial cross section $\sigma^{\Sigma^-}_{A0}(\omega)$ for population of the $A\ ^1\Pi(v'=0)$ level via the $^2\Sigma^-$ intermediate state is very small compared with the $\sigma^{\Delta}_{A0}(\omega)$ and $\sigma^{\Sigma^+}_{A0}(\omega)$ ones, which is due the very low Auger rate $\Gamma^A_{\pi^*(\Sigma^-)}$ in comparison with the $\Gamma^A_{\pi^*(\Delta)}$ and $\Gamma^A_{\pi^*(\Sigma^+)}$ rates. This results in a dip in the total cross sections $\sigma_{Av'}(\omega)$ for population of the $A\ ^1\Pi(v')$ levels via the N*O resonance which is situated between two maxima. Since the order of the electronic states for the NO* resonance is different the above dip in the total population cross section is in this case located on the low energy side of the two maxima.

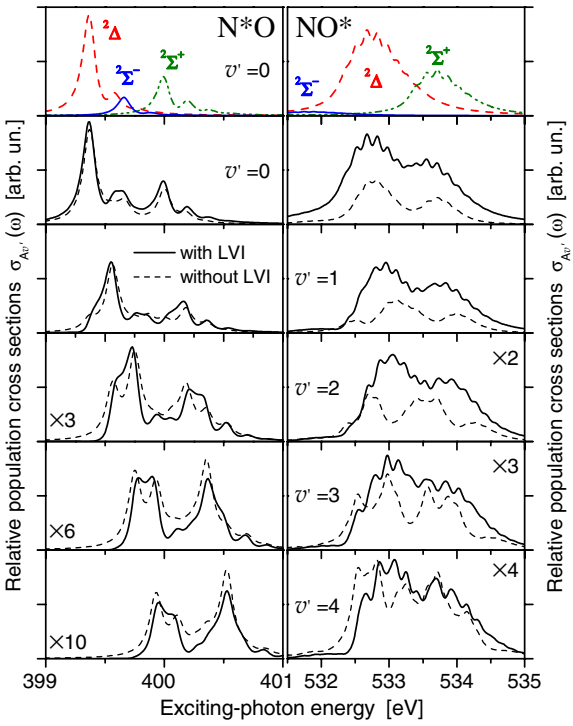

Fig. 5. Total cross sections for population (6) of the $A\ ^1\Pi(v')$ vibrational levels via the N*O and NO* resonances computed with (solid line) and without (dashed line) taking into account the LVI. In both N*O and NO* cases (for the $v'=0$ vibrational level only) the uppermost panels illustrate the partial cross sections (8) for the $^2\Delta$ (dash), $^2\Sigma^-$ (solid), and $^2\Sigma^+$ (dash-dot-dot) states.

One can see from the left panels of Figure 5 that both maxima in the total population of the $A\ ^1\Pi(v')$ vibrational levels via the N*O resonance are permanently shifted toward larger exciting-photon energies with increasing v' quantum number. This is due to the fact that the potential energy curves for the NO^+ A $^1\Pi$ state and for the core-excited N*O electronic states are very similar at the respective equilibrium internuclear distances (cf. value of $\omega_e(A\ ^1\Pi) \approx 199$ meV with ω_e(N*O) ≈ 195 meV and value of $r_e(A\ ^1\Pi) = 1.19$ Å with r_e(N*O) ≈ 1.21 Å, listed in Tabs. 2 and 3). Therefore, the Franck-Condon factors for Auger decay $|\langle v'|v_r\rangle|^2$ are approximately diagonal and high vibrational levels v' of the $A\ ^1\Pi$ state are mainly populated via high vibrational levels v_r of the N*O resonance. This argumentation is not true for the NO* intermediate states and, therefore, the above shift is not as obvious from the right panels of Figure 5.

One can also see from Figure 5 that the influence of the LVI on the computed cross sections for population of the $A\ ^1\Pi(v')$ states via the intermediate N*O resonance is not very large. This holds because the vibrational spacing of 195 meV is about 1.5 times larger than the natural width of 124 meV of the N*O resonance [9]. On the other hand, the areas and shapes of the $\sigma_{Av'}(\omega)$ calculated with and without LVI for the NO* resonance are very different because its natural width of 170 meV is already larger than

Table 4. Relative integrated cross sections (12) for total population of the $A(v' \leq 4)$ vibrational levels via the N^*O and NO^* resonances calculated in different approximations. The sum over the v' index of the direct population cross sections (lines 'a' and 'b') is normalized to 100%.

Sate	$A(v')$						
Level	0	1	2	3	4	...	Sum
N^*O [a]	34.8	29.2	18.1	9.7	4.7	...	100
N^*O [b]	42.4	29.2	15.3	7.4	3.4	...	100
N^*O [c]	146	53.2	23.7	10.2	4.2	...	240
NO^* [a]	9.3	7.7	6.4	6.2	6.7	...	100
NO^* [b]	24.2	17.3	11.4	8.5	6.9	...	100
NO^* [c]	239	94.2	43.3	20.5	10.5	...	436

[a] Lifetime vibrational interference is neglected; [b] lifetime vibrational interference is accounted for; [c] cascade population via radiative decay of the $A'\ ^1\Sigma^-$ and $W\ ^1\Delta$ states is accounted for.

the vibrational spacing of 150 meV [10]. In order to illustrate the interference effects quantitatively, we introduced the integral cross sections, $\bar{\sigma}_{Av'}$, for total population of the $A\ ^1\Pi(v')$ vibrational levels via the $1s^{-1}\pi^*$ resonance:

$$\bar{\sigma}_{Av'} = \int_{\omega_1}^{\omega_2} \sigma_{Av'}(\omega)\, \mathrm{d}\omega, \qquad (12)$$

where the integration is performed within the present exciting-photon energy range similar to equation (2). Relative values of the $\bar{\sigma}_{Av'}$ computed in the different approximations for the $v' \leq 4$ vibrational levels relevant to the present measurements are listed in Table 4. The sum of the direct integral population cross sections over v' is normalized to 100%. From this table one can recognize that LVI transfers the integral population of the $A\ ^1\Pi(v')$ states from higher to lower v' vibrational quantum numbers.

The accuracy of computing the population $\sigma_{\Lambda'\Sigma'v'}(\omega)$ was tested by calculating the Auger spectra of the resonantly excited NO molecule measured in [14,15]. The presently computed participator $1s^{-1}\pi^* \rightarrow X\ ^1\Sigma^+$ Auger spectra of the N^*O and NO^* molecules (not shown in the present paper) are in good agreement with the theoretical and experimental data from [14,15]. The overall agreement between the presently computed total spectra for the spectator $1s^{-1}\pi^* \rightarrow \Lambda\Sigma$ Auger decay and the spectra from [14] is satisfactory. However, for some partial spectator Auger spectra discrepancies between the spectra computed by [14] and ours exist. This can be related to the different potential curves and partial Auger rates used in our paper and in [14] (in [14], Morse potentials and Auger rates were adjusted in order to fit the experimental spectra).

4.2 Cross sections for the A → X fluorescence

The relative values of presently measured cross sections for the $A\ ^1\Pi(v') \rightarrow X\ ^1\Sigma^+(v'')$ fluorescence $\sigma_{Av'}^{Xv''}(\omega)$ are shown in Figure 6 whereas the experimental doubly integrated cross sections $\bar{\sigma}_{Av'}^{Xv''}$ are listed in Table 5.

Table 5. Doubly integrated cross sections $\bar{\sigma}_{Av'}^{Xv''}$ (2) observed for the $A(v') \rightarrow X(v'')$ fluorescence of the NO^+ ion after Auger decay of the $1s^{-1}\pi^*$ resonance of N^*O and NO^* and calculated in the different approximations (relative to the $\bar{\sigma}_{A1}^{X1}$ in %).

	N^*O				NO^*			
Band	a)	b)	c)	d)	a)	b)	c)	d)
4–0	24	17	12	8(1)	131	60	17	13(2)
3–0	44	34	25	22(4)	107	65	29	30(7)
2–0	59	50	42	35(8)	79	63	44	36(8)
3–1	15	12	9	12(2)	37	23	10	20(4)
1–0	50	50	50	40(8)	50	50	50	44(8)
2–1	57	49	41	41(2)	77	61	43	39(4)
0–0	17	21	39	24(1)	17	20	36	22(2)
1–1	100	100	100	100	100	100	100	100
2–2	4.9	4.1	4	4(1)	7	5	4	
0–1	61	74	140	117(5)	61	71	129	123(6)

[a] Theory: lifetime vibrational interference is neglected; [b] theory: lifetime vibrational interference is accounted for; [c] theory: cascade population of the $A\ ^1\Pi$ state via radiative decay of the $A'\ ^1\Sigma^-$ and $W\ ^1\Delta$ states is accounted for; [d] experiment: data corrected for the QE of CsI detector.

The values of $\bar{\sigma}_{A1}^{X1}$ for the prominent and well separated $A(v'=1) \rightarrow X(v''=1)$ band (line No. 19) were set in Table 5 to 100%. Ambiguous separation of observed overlapping lines and background fluorescence emission results in the error bars listed together with measured values of the $\bar{\sigma}_{Av'}^{Xv''}$. Experimental cross sections $\sigma_{Av'}^{Xv''}(\omega)$ for the bands 2–0 (line no 12), 3–1 (line no 14), 1–0 (line no 15) and 0–0 (line no 18), although resolved in the present experiment, are not shown in the right panels of Figure 6 due to the low count rate (signal-to-noise ratio) in the NO^* case (see also Fig. 2b), whereas the 2–2 band (line No. 20) in this case was not resolved.

In order to calculate cross sections for the $A\ ^1\Pi(v') \rightarrow X\ ^1\Sigma^+(v'')$ fluorescence we computed the radiative widths $\Gamma_{Av'}^{Xv''}$ and fluorescence yields $\chi_{Av'}^{Xv''}$. In computing the fluorescence yield via equation (10) we neglected the possible $A\ ^1\Pi \rightarrow A'\ ^1\Sigma^-$ and $A\ ^1\Pi \rightarrow W\ ^1\Delta$ transitions which have negligibly low probability compared with the $A\ ^1\Pi \rightarrow X\ ^1\Sigma^+$ fluorescence due to the small transition energy factor $(\lambda_{v'v''})^{-3}$ entering equation (11). The partial fluorescence widths $\Gamma_{Av'}^{Xv''}$ for the $A(v') \rightarrow X(v'')$ transitions were computed in the present work with accounting for the dependence of the electron transition moment $\mathbf{D}_A^X(R)$ on the internuclear distance via equation (11).

Computed cross sections $\sigma_{Av'}^{Xv''}(\omega)$ for the $A\ ^1\Pi(v') \rightarrow X\ ^1\Sigma^+(v'')$ fluorescence excited via N^*O and NO^* resonances are compared with available experimental cross sections in Figure 6. For a better comparison with experiment the cross sections computed via equation (5) were additionally convolved with Gaussians of 100 meV and 135 meV FWHM for the N^*O and NO^* excitations, respectively. In order to facilitate comparison of the exciting-photon energy dependencies we equalized the respective areas of computed and measured cross sections $\sigma_{Av'}^{Xv''}(\omega)$. One can see from Figure 6 that the shapes of

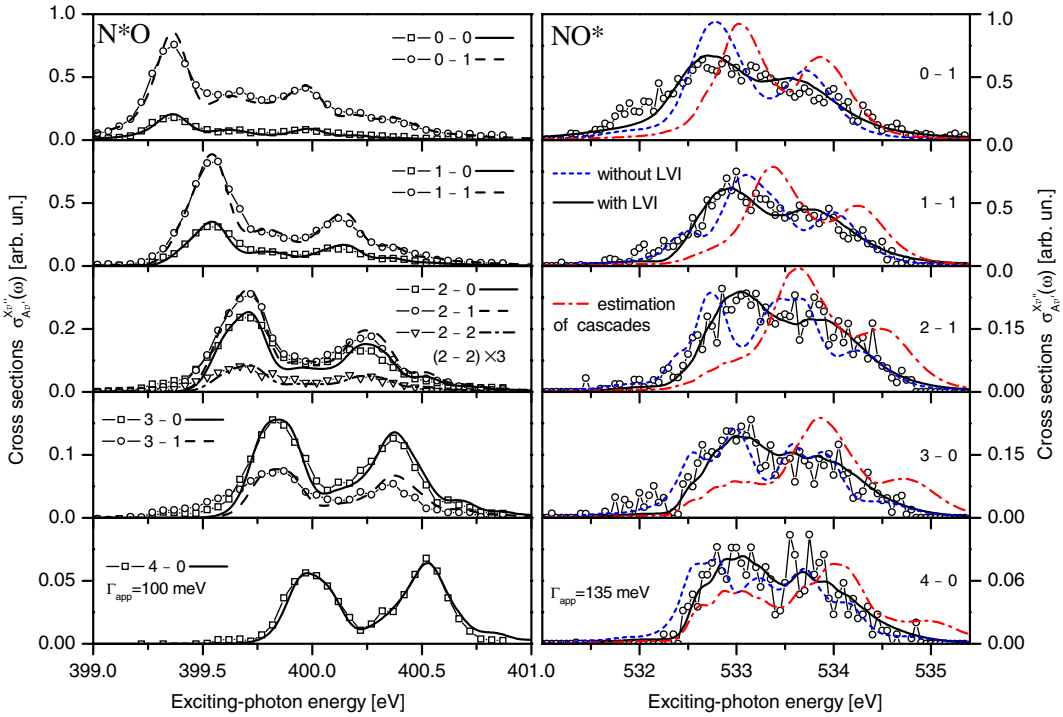

Fig. 6. (Color online) Comparison between presently measured and computed cross sections for the $A\ ^1\Pi(v') \rightarrow X\ ^1\Sigma^+(v'')$ fluorescence excited via the N*O and NO* resonances. Cross sections computed via equation (5) were additionally convolved with Gaussians of 100 meV and 135 meV FWHM, respectively. For better comparison of shapes the areas of computed cross section were set equal to the respective areas of the measured ones whereas the doubly integrated cross sections $\bar{\sigma}_{Av''}^{Xv''}$ (2) are compared in Table 5. For the NO* case the fluorescence cross sections calculated neglecting the LVI are shown by short-dash lines and those estimated with additional cascade population of the $A\ ^1\Pi$ state via radiative decay of the $A'\ ^1\Sigma^-$ and $W\ ^1\Delta$ states by dash-dot lines.

the computed $\sigma_{Av'}^{Xv''}(\omega)$ agree very well with the shapes of the measured ones. From equation (5) it is evident that the energy dependence of the fluorescence emission cross sections $\sigma_{Av'}^{Xv''}(\omega)$ originates from the energy dependence of the cross sections $\sigma_{Av'}(\omega)$ for total population of the $A\ ^1\Pi(v')$ states. Therefore, dips in the fluorescence intensities observed for the $A(v') \rightarrow X(v'')$ bands occur due to the small Auger rate $\Gamma^A_{\pi^*(\Sigma^-)}$ compared with the $\Gamma^A_{\pi^*(\Sigma^+)}$ and $\Gamma^A_{\pi^*(\Delta)}$ rates (see also discussion in Sect. 4.1).

Fluorescence cross sections calculated neglecting the LVI are shown in the right panels of Figure 6 for the NO* case by short-dash lines. One can see that accounting for the LVI changes the exciting-photon energy dependencies of the calculated $\sigma_{Av'}^{Xv''}(\omega)$ and improves the agreement between theory and experiment noticeably. Unfortunately, the influence of the LVI on the calculated cross sections in case of the N*O excitation cannot be tested experimentally due to the present exciting-photon resolution and, therefore, was not represented in Figure 6.

The relative values of doubly integrated cross sections $\bar{\sigma}_{Av'}^{Xv''}$ calculated in different approximations are compared in Table 5 with measured ones. The experimental values of the $\bar{\sigma}_{A0}^{X1}$ in both, N*O and NO*, cases are larger than the theoretical ones since the 1–0 fluorescence band in the present measurements cannot be separated from the NI atomic line and the 3–3 band (see line No. 21 in Tab. 1). One can see from Table 5 that accounting for the LVI changes the computed values of $\bar{\sigma}_{Av'}^{Xv''}$ (small changes in the N*O and large ones in the NO* cases) and definitely improve the agreement between computed and measured doubly integrated cross sections. For instance, accounting for the LVI decreases the computed values of $\bar{\sigma}_{A4}^{X0}$ and $\bar{\sigma}_{A3}^{X0}$ in the NO* case by the factors of 2.2 and 1.7, respectively. However, in both the N*O and NO* cases the differences between computed 'columns *b*)' and measured 'columns *d*)' values of the $\bar{\sigma}_{Av'}^{Xv''}$ are still remarkable. To some extent this disagreement can be related to the fact that we measure the fluorescence from the aligned $A\ ^1\Pi(v')$ states whereas the computed fluorescence refers to isotropic states. An investigation of the $A\ ^1\Pi \rightarrow X\ ^1\Sigma^+$ fluorescence anisotropy is planned to be done in the future.

4.3 Cascade population of the A $^1\Pi$ state

In this section we estimate the influence of possible cascade processes in the NO^+ ion on the measured $A\ ^1\Pi \rightarrow X\ ^1\Sigma^+$ fluorescence emission cross sections. The energy level diagram describing some singlet and triplet states of the NO^+ ion is shown in Figure 7. Since the probability for predissociation is usually by several orders of magnitude larger than the radiative decay probability [51] we restricted our consideration to singlet and triplet states of

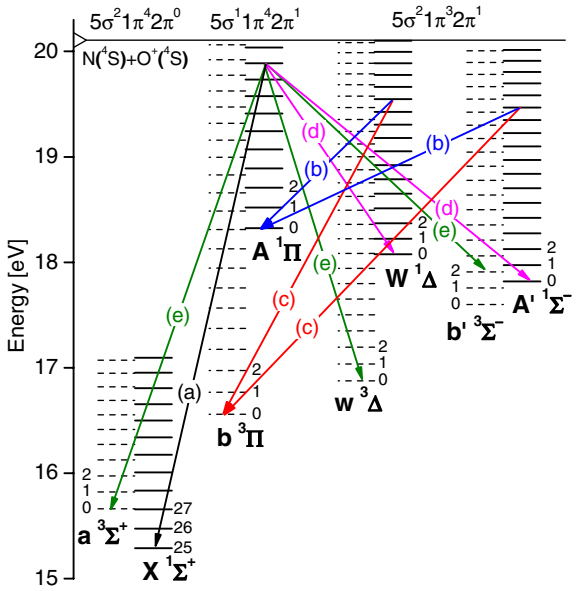

Fig. 7. (Color online) Scheme of radiative cascades in the NO^+ ion: (a) $A\ ^1\Pi \rightarrow X\ ^1\Sigma^+$ fluorescence; (b) cascade population of the $A\ ^1\Pi$ state via radiative decay of the $A'\ ^1\Sigma^-$ and $W\ ^1\Delta$ states; (c) de-population of the $A'\ ^1\Sigma^-$ and $W\ ^1\Delta$ states via spin forbidden transitions to the $b\ ^3\Pi$ state; (d) and (e) de-population of the $A\ ^1\Pi$ state via radiative transition to the $A'\ ^1\Sigma^-$ and $W\ ^1\Delta$ states and spin forbidden transitions to the $b'\ ^3\Sigma^-$, $w\ ^3\Delta$ and $a\ ^3\Sigma^+$ states. The energy positions of the vibrational levels of the NO^+ states were obtained using experimental data from [46].

the NO^+ ion lying below the first $N(^4S)+O^+(^4S)$ dissociation limit (20.107 eV [19,52]). The $^{1,3}\Pi$ and $^{1,3}\Delta,\Sigma^-$ states of the NO^+ ion have a relatively strong population via the $1s\varepsilon\lambda - 5\sigma 2\pi$ and $1s\varepsilon\lambda - 1\pi 2\pi$ participator Auger decays of the $1s^{-1}\pi^*$ resonance [18]. One can see from this diagram that higher vibrational levels of the $A'\ ^1\Sigma^-$ and $W\ ^1\Delta$ states can (if energetically possible) additionally populate the $A\ ^1\Pi(v')$ states via radiative transitions '(b)', which in the pure $\Lambda\Sigma$-coupling scheme are the only deexcitation channels for the A' and W singlet states. Therefore, radiation cascades will transfer population of the $A'\ ^1\Sigma^-$ and $W\ ^1\Delta$ states to the $A\ ^1\Pi(v')$ levels (basically to the lower v' quantum numbers due to the transition energy factor).

It is difficult to estimate the individual populations of the $A'\ ^1\Sigma^-$ and $W\ ^1\Delta$ states on the basis of the experimental Auger spectra due to the overlapping between lines belonging to different valence-ionized states, as mentioned in the introduction. Therefore, the total cross sections for populating the $A\ ^1\Pi(v')$ states, $\sigma^c_{Av'}(\omega)$, which account for the direct and additional cascade transitions, were calculated in the present paper as:

$$\sigma^c_{Av'}(\omega) = \sigma_{Av'}(\omega) + \sum_{K'',v''} \sigma_{K''v''}(\omega)\ \chi^{Av'}_{K''v''}, \qquad (13)$$

where $\sigma_{K''v''}(\omega)$ are cross sections for population of the $K''(v'')$ states via Auger decay of the $1s^{-1}\pi^*$ resonance, and $\chi^{Av'}_{K''v''}$ is the yield for $K''(v'') \rightarrow A\ ^1\Pi(v')$ fluorescence emission. In the subsequent calculations we neglect a possible spin-orbit coupling between singlet and triplet states of the NO^+ ion. This restricts: (i) possible K'' states populating the $A\ ^1\Pi$ state to the $A'\ ^1\Sigma^-$ and $W\ ^1\Delta$ states only; and (ii) possible de-excitation channels for the $A'\ ^1\Sigma^-$ and $W\ ^1\Delta$ states to the $A\ ^1\Pi$ state only.

Relative values of integral population cross sections $\bar{\sigma}^c_{Av'}$ calculated via equations (13) and (12) are listed in the lines 'c)' of Table 4. One can see from this table, that radiative transitions from the $A'\ ^1\Sigma^-$ and $W\ ^1\Delta$ states increase the population of the $A\ ^1\Pi$ states strongly, especially for lower v' levels. The ratios of population cross sections calculated with and without accounting for the cascade processes, $\bar{\sigma}^c_{Av'}/\bar{\sigma}_{Av'}$, are: 3.4, 1.8 and 1.6 for the $v' = 0$, 1 and 2 levels in the case of the N*O excitation and 9.9, 5.4 and 3.8 for the $v' = 0$, 1 and 2 levels in the case of the NO* excitation. As a result, exciting-photon energy dependencies of the theoretical population cross sections $\sigma^c_{Av'}(\omega)$ and, consequently, of the fluorescence emission cross sections $\sigma^{Xv''}_{Av'}(\omega)$ are determined mainly by the energy dependencies of the cross sections for population of the $A'\ ^1\Sigma^-$ and $W\ ^1\Delta$ states via the $1s^{-1}\pi^*$ resonance. This fact is demonstrated in the right panels of Figure 6 for the NO* case only. One can see that the exciting-photon energy dependencies of the fluorescence emission cross sections $\sigma^{Xv''}_{Av'}(\omega)$ calculated with accounting for the radiation cascades (dash-dot lines) differ from the measured ones.

The relative doubly integrated cross sections for the $A\ ^1\Pi(v') \rightarrow X\ ^1\Sigma^+(v'')$ fluorescence calculated with accounting for the radiative transitions from the $A'\ ^1\Sigma^-$ and $W\ ^1\Delta$ states are listed in the columns 'c)' of Table 5. One can recognize from this table, that the above cascade transitions bring the relative values of calculated cross sections $\bar{\sigma}^{Xv''}_{Av'}$ in a better agreement with the experimental ones. Indeed, dipole transitions from the $A'\ ^1\Sigma^-$ and $W\ ^1\Delta$ states decrease the relative cross sections for the fluorescence from higher v' vibrational levels of the $A\ ^1\Pi$ state which, in turn, is due to the strong increase of the total population of lower v' levels. Thus, radiation cascades improves the agreement between the theoretical and experimental doubly integrated cross sections $\bar{\sigma}^{Xv''}_{Av'}$ but deteriorate the agreement between the calculated and measured exciting-photon energy dependencies of the $\sigma^{Xv''}_{Av'}(\omega)$.

In order to reduce the dominating cascade population of the $A\ ^1\Pi$ state via radiative transitions from the $A'\ ^1\Sigma^-$ and $W\ ^1\Delta$ states we suggest a substantial spin-orbit coupling between the singlet and triplet states of the NO^+ ion. This makes possible the $A'\ ^1\Sigma^- \rightarrow b\ ^3\Pi$ and $W\ ^1\Delta \rightarrow b\ ^3\Pi$ spin forbidden dipole transitions (marked by '(c)' in scheme 7) which can be observed in the visible range approximately between 500 and 950 nm. The suggested coupling is supported by the measurements of [20] where the fluorescence from the $b\ ^3\Pi \rightarrow X\ ^1\Sigma^+$ triplet–singlet transitions has been clearly observed. In addition, we propose mechanisms for the de-population of higher v' vibrational levels of the $A\ ^1\Pi$ state which could bring the theoretical doubly integrated cross sections for the $A\ ^1\Pi \rightarrow X\ ^1\Sigma^+$ fluorescence in a better agreement with the experimental ones and will not influence the

exciting-photon energy dependencies of the calculated fluorescence cross sections $\sigma_{Av'}^{Xv''}(\omega)$. These mechanisms are: the $A\ ^1\Pi \rightarrow A'\ ^1\Sigma^-$ and $A\ ^1\Pi \rightarrow W\ ^1\Delta$ transitions '(d)' in scheme 7 and the $A\ ^1\Pi \rightarrow b'\ ^3\Sigma^-$, $A\ ^1\Pi \rightarrow w\ ^3\Delta$ and $A\ ^1\Pi \rightarrow a\ ^3\Sigma^+$ transitions '(e)' neglected in the present calculations of the $A\ ^1\Pi \rightarrow X\ ^1\Sigma^+$ fluorescence yield. The above singlet–singlet transitions manifest themselves as a fluorescence in the infrared wavelength region, whereas the singlet–triplet fluorescence can be observed in the visible range between 400 and 800 nm. In order to take all the above population and de-population pathways into account, precise calculations of absolute fluorescence rates for the (a)–(e) transitions in scheme 7 are required.

From the experimental point of view, in order to estimate the real influence of the radiation cascade processes on the observed $A\ ^1\Pi \rightarrow X\ ^1\Sigma^+$ fluorescence, one needs to measure the ratio of integral cross sections for populating the $A\ ^1\Pi(v'=0)$ and $A\ ^1\Pi(v'=1)$ states. From Table 4 it is evident that the ratios $\bar{\sigma}_{A0}/\bar{\sigma}_{A1}$ (lines '*b*)') are equal to 1.5 for the N*O and 1.4 for the NO* cases, whereas the ratios $\bar{\sigma}^c_{A0}/\bar{\sigma}^c_{A1}$ (lines '*c*)') are equal to 2.7 and 2.5, respectively. Unfortunately, in the present experiment, none of the above theoretical ratios could be tested since the observed transitions from the $A\ ^1\Pi(v'=0)$ state are either too weak (0–0 band) or were not separated from the other lines (0–1 band). Therefore, an additional experimental information on the most intensive and well separated 1–2, 0–2, 0–3, 0–4, 1–5, 0–5 and 1–6 bands of the NO^+ $\left(A\ ^1\Pi \rightarrow X\ ^1\Sigma^+\right)$ system excited via the $1s^{-1}\pi^*$ resonance is of considerable interest. These bands can be observed between 140 and 180 nm [20]. Both, precise calculations of the radiative cascade transitions in the NO^+ ion and the experimental investigation of the extended fluorescence wavelength interval are the subjects of a forthcoming paper.

5 Summary

Cross sections for the excitation of fluorescence in the wavelength range between 118 and 142 nm were measured for the nitric oxide by photon-induced fluorescence spectroscopy as functions of the exciting-photon energy between 398.95 eV and 400.85 eV and between 530.90 eV and 535.45 eV, corresponding to the N*O and NO* resonances, respectively. Resolution of the exciting-photon radiation was set to 100 meV and 135 meV FWHM at 400 eV and 530 eV, respectively. The fluorescence resolution was $\Delta\lambda_{fl} = 0.2$ nm. The observed fluorescence is dominated by transitions in the neutral and charged N and O fragments and by $A\ ^1\Pi(v') \rightarrow X\ ^1\Sigma^+(v'')$ vibrational bands of the NO^+ ion. In order to explain the observed cross sections for $A \rightarrow X$ fluorescence emission we computed the potential energy curves for the molecular states involved in the considered process. The molecular constants computed for these states are in good agreement with the experimental data. The photoionization spectra computed for the N*O and NO* intermediate states are also in good agreement with the measured ones.

Cross sections for the $A\ ^1\Pi(v') \rightarrow X\ ^1\Sigma^+(v'')$ fluorescence were computed in the present paper with taking into account the lifetime vibrational interference between pathways connected with different $1s^{-1}\pi^*\,(v_r)$ vibrational levels. It was demonstrated that the complex dependencies of the measured cross sections for the $A \rightarrow X$ fluorescence on the exciting-photon energy and on both v' and v'' vibrational quantum numbers are due to the small Auger rate for the $^2\Sigma^-$ intermediate N*O and NO* core-excited state compared with the rates for the $^2\Delta$ and $^2\Sigma^+$ states and due to the lifetime vibrational interference (very strong in the NO* case). In order to reduce the remaining difference between calculated and measured doubly integrated fluorescence cross sections the additional cascade populations of the $A\ ^1\Pi$ state via radiative transitions from the $W\ ^1\Delta$ and $A'\ ^1\Sigma^-$ states were estimated. It was obtained that the cascade transitions improve the agreement between calculated and measured doubly integrated cross sections $\bar{\sigma}_{Av'}^{Xv''}$ and simultaneously deteriorate the agreement between the exciting-photon energy dependencies of the calculated and measured $\sigma_{Av'}^{Xv''}(\omega)$.

The discrepancy between the energy dependencies of the cross sections calculated with accounting for the radiative cascade transitions and the measured fluorescence emission cross sections led us to infer a significant spin-orbit coupling between singlet and triplet states of the NO^+ ion which makes possible spin forbidden dipole transitions. A more accurate interpretation of the present experiment requires a detailed theoretical study of the radiative cascade processes in the NO^+ ion including the spin forbidden dipole transitions and measurements of the $A\ ^1\Pi(v') \rightarrow X\ ^1\Sigma^+(v'')$ fluorescence excited via the N*O and NO* resonances in an extended wavelength range up to 180 nm.

This work has been supported by the Deutsche Forschungsgemeinschaft (DFG), by the Bundesministerium für Bildung und Forschung (BMBF) (Förderkennzeichen 05 ES3XBA/5), and by the Russian Foundation for Basic Research (grant No. 07-03-00876). VLS appreciates support from the Southern Federal University (grant No. 182). The cooperation between the groups at the universities of Kaiserslautern and Rostov-on-Don was supported by the Alexander-von-Humboldt foundation within the framework of an institute partnership with funds from BMBF. The authors are grateful to the BESSY staff for support during the experiments, particularly to Drs Gerd Reichard and Rolf Follath. PhVD and VLS would like to thank the Department of Physics, Kaiserslautern University of Technology and Institute of Physics, University of Kassel for the hospitality during their stay there.

References

1. F.K. Gel'Mukhanov, L.N. Mazalov, A.V. Kondratenko, Chem. Phys. Lett. **46**, 133 (1977)
2. F. Gel'mukhanov, H. Ågren, Phys. Rep. **312**, 87 (1999)
3. K.C. Prince, M. Vondráček, J. Karvonen, M. Coreno, R. Camilloni, L. Avaldi, M. de Simone, J. Electr. Spectr. Relat. Phenom. **101–103**, 141 (1999)

4. M. Neeb, J.E. Rubensson, M. Biermann, W. Eberhardt, J. Electr. Spectr. Relat. Phenom. **67**, 261 (1994)
5. C.T. Chen, Y. Ma, F. Sette, Phys. Rev. A **40**, 6737 (1989)
6. A. Marquette, M. Meyer, F. Sirotti, R.F. Fink, J. Phys. B: At. Mol. Opt. Phys. **32**, L325 (1999)
7. A. Ehresmann, L. Werner, S. Klumpp, S. Lucht, H. Schmoranzer, S. Mickat, R. Schill, K.H. Schartner, Ph.V. Demekhin, M.P. Lemeshko, V.L. Sukhorukov, J. Phys. B: At. Mol. Opt. Phys. **39**, 283 (2006)
8. A. Ehresmann, L. Werner, S. Klumpp, Ph.V. Demekhin, M.P. Lemeshko, V.L. Sukhorukov, K.H. Schartner, H. Schmoranzer, J. Phys. B: At. Mol. Opt. Phys. **39**, L119 (2006)
9. H. Wang, R.F. Fink, M.N. Piancastelli, I. Hjelte, K. Wiesner, M. Bässler, R. Feifel, O. Björneholm, C. Miron, A. Giertz, F. Burmeister, S.L. Sorensen, S. Svensson, J. Phys. B: At. Mol. Opt. Phys. **34**, 4417 (2001)
10. R. Püttner, I. Domingue, T.J. Morgan, C. Cisneros, R.F. Fink, E. Rotenberg, T. Warwick, M. Domke, G. Kaindl, A.S. Schlachter, Phys. Rev. A **59**, 3415 (1999)
11. T.X. Carroll, S.E. Anderson, L. Ungier, T.D. Thomas, Phys. Rev. Lett. **58**, 867 (1987)
12. T.X. Carroll, T.D. Thomas, J. Chem. Phys. **97**, 894 (1992)
13. T.X. Carroll, M. Coville, P. Morin, T.D. Thomas, J. Chem. Phys. **101**, 998 (1994)
14. E. Kukk, G.S.J.D. Bozek, W.T. Cheng, N. Berrah, Phys. Rev. A **63**, 062702 (2001)
15. H. Wang, R.F. Fink, M.N. Piancastelli, M. Bässler, I. Hjelte, O. Björneholm, F. Burmeister, R. Feifel, A. Giertz, C. Miron, S.L. Sorensen, K. Wiesnera, S. Svensson, Chem. Phys. **289**, 31 (2003)
16. P. Erman, P.A. Hatherly, A. Karawajczyk, E.R.K.U. Köbley, M. Stankiewicz, K.Y. Franzén, J. Phys. B: At. Mol. Opt. Phys. **29**, 1501 (1996)
17. S.W. Yu, W.C. Stolte, G.Ö. R. Guillemin, I.C. Tran, M.N. Piancastelli, R. Feng, D.W. Lindle, J. Phys. B: At. Mol. Opt. Phys. **37**, 3583 (2004)
18. R. Fink, J. Chem. Phys. **106**, 4038 (1997)
19. K.P. Huber, G. Herzberg, *Molecular Spectra and Molecular Structure. IV. Constants of Diatomic Molecules* (Van Nostrand Reinhold Comp., New York, 1979)
20. W.B. Maier II, R.F. Holland, J. Chem. Phys. **54**, 2693 (1971)
21. F.R. Gilmore, J. Quant. Spectr. Radiat. Transf. **5**, 369 (1965)
22. P. Baer, E. Miescher, Nature **169**, 581 (1952)
23. Y. Tanaka, J. Chem. Phys. **21**, 562 (1953)
24. P. Baer, E. Miescher, Helv. Phys. Acta **26**, 91 (1953)
25. E. Miescher, Can. J. Phys. **33**, 355 (1955)
26. E. Miescher, Helv. Phys. Acta **29**, 135 (1956)
27. R.W. Field, J. Mol. Spectrosc. **47**, 194 (1973)
28. F. Alberti, A.E. Douglas, Can. J. Phys. **53**, 1179 (1975)
29. O. Edqvist, L. Åsbrink, E. Lindholm, Z. Naturforsch. **26a**, 1407 (1971)
30. P. Natalis, J. Delwiche, J.E. Collin, G. Caprace, M.T. Praet, Phys. Scripta **16**, 242 (1971)
31. S.H. Southworth, A.C. Parr, J.E. Hardis, J.L. Dehmer, J. Chem. Phys. **87**, 5125 (1987)
32. H. Park, R.N. Zare, J. Chem. Phys. **99**, 6537 (1999)
33. P. Erman, A. Karawajczyk, E. Rachlew-Källne, C. Strömholm, J. Chem. Phys. **102**, 3064 (1995)
34. E.W. Thulstrup, E. Öhrn, J. Chem. Phys. **57**, 3716 (1972)
35. P.W. Thulstrup, E.W. Thulstrup, A. Andersen, E. Öhrn, J. Chem. Phys. **60**, 3975 (1974)
36. H. Liebel, A. Ehresmann, H. Schmoranzer, Ph.V. Demekhin, B.M. Lagutin, V.L. Sukhorukov, J. Phys. B: At. Mol. Opt. Phys. **35**, 895 (2002)
37. A. Ehresmann, H. Liebel, H. Schmoranzer, B. Zimmermann, S. Kammer, K.H. Schartner, Ph.V. Demekhin, V.L. Sukhorukov, J. Phys. B: At. Mol. Opt. Phys. **36**, 3669 (2003)
38. A. Ehresmann, L. Werner, S. Klumpp, H. Schmoranzer, Ph.V. Demekhin, B.M. Lagutin, V.L. Sukhorukov, S. Mickat, S. Kammer, B. Zimmermann, K.H. Schartner, J. Phys. B: At. Mol. Opt. Phys. **37**, 4405 (2004)
39. H. Schmoranzer, R. Zietz, Phys. Rev. A **18**, 1472 (1978)
40. H. Schmoranzer, K. Molter, T. Noll, J. Imschweiler, Nucl. Instrum. Meth. Phys. Res. A **246**, 485 (1986)
41. H. Schmoranzer, H. Liebel, F. Vollweiler, R. Müller-Albrecht, A. Ehresmann, K.H. Schartner, B. Zimmermann, Nucl. Instrum. Meth. Phys. Res. A **467–468**, 1526 (2001)
42. R.L. Kelly, J. Phys. Chem. Ref. Data **16** (Suppl. 1), 1 (1987)
43. I.I. Sobelman, *Introduction to the theory of atomic spectra*, 1st edn. (Pergamon Press, Oxford - New York - Toronto, 1972)
44. M.W. Schmidt, K.K. Baldridge, J.A. Boatz, S.T. Elbert, M.S. Gordon, J.J. Jensen, S. Koseki, N. Matsunaga, K.A. Nguyen, S. Su, T.L. Windus, M. Dupuis, J.A. Montgomery, J. Comput. Chem. **14**, 1347 (1993)
45. T.H. Dunning Jr, J. Chem. Phys. **55**, 716 (1971)
46. D.L. Albritton, A.L. Schmeltekopf, J. Chem. Phys. **71**, 3271 (1979)
47. K. Lee, D.Y. Kim, C.I. Ma, D.M. Hanson, J. Chem. Phys. **100**, 8550 (1994)
48. N. Kosugi, J. Adachi, E. Shigemasa, A. Yagishita, J. Chem. Phys. **97**, 8842 (1992)
49. G. Remmers, M. Domke, A. Puschmann, T. Mandel, G. Kaindl, E. Hudson, D.A. Shirley, Chem. Phys. Lett. **214**, 241 (1993)
50. E.J. McGuire, Phys. Rev. **185**, 1 (1969)
51. H. Lefebvre-Brion, R.W. Field, *Perturbations in the spectra of diatomic molecules*, 1st edn. (Academic Press, London-Orlando, 1986)
52. C.E. Moore, *Atomic Energy Levels* (US Govt Printing Office, Washington, DC, 1971), NBS Circular No. 467